Alternately Arranged Segmented Transmitter Pads With Magnetic Field Complementation for Suppressing Power Fluctuation in Dynamic Wireless Power Transfer

Hai Xu, *Graduate Student Member, IEEE*, and Zhicong Huang, *Senior Member, IEEE*

***Abstract*—Dynamic wireless power transfer (DWPT) is a promising solution to address driving range anxiety or eliminate necessity of carrying heavy batteries for electric vehicles (EVs). The DWPT systems are expected to operate satisfactorily with a stable output characteristic over a wide driving range. In this article, a novel transmitter (Tx) track is proposed, which is based on alternately arranged segmented rectangular-solenoid pads. Such a Tx track features magnetic field complementation to suppress the fluctuation of output on the receiver (Rx) side against the wide-range and dynamic displacement. The proposed design allows the Tx and Rx pads to have a uniform size, such that the coupling coefficient can be maximized for optimal power transfer capability for a given copper usage and ferrite core. It also allows a wide distance between the adjacent transmitter pads, which further enables the reduction of copper and ferrite core usage and alleviates the cross-coupling issues. In addition, a novel DWPT system with an orthogonal excitation method based on the proposed Tx track is developed, along with a detailed parameter design methodology. The operation of the proposed DWPT system is purely passive and highly robust, without any necessity for sensing and active control. A 1 kW DWPT experimental prototype is built to verify the proposed DWPT design.**

***Index Terms*—Alternate arrangement, dynamic wireless power transfer (DWPT), magnetic field complementation, power fluctuation suppression, segmented transmitter pads.**

I. Introduction

NOWADAYS, electric vehicles (EVs) have gained widespread adoption as part of the global effort to promote sustainable and environmentally friendly transportation. EVs are typically equipped with large, heavy, and expensive batteries, but they still face driving range and charging speed anxieties [1]. Dynamic wireless power transfer (DWPT) is a potential solution to address these issues by allowing EVs to acquire power while in motion on the road [2].

To suppress power fluctuation in the DWPT process, a magnetic coupler with a consistent coupling coefficient regardless of the dynamic displacement can be designed and used. According to the transmitter length, the transmitter (Tx) pad of the magnetic couplers in the DWPT systems can be classified into long-track type [3], [4], [5] and segmented type [6], [7], [8]. The length of the long-track Tx pad is significantly larger than that of the receiver (Rx) pad [9]. In this way, a consistent coupling coefficient between the Tx and Rx pads can be readily achieved over a wide-range displacement. Some well-known long-track Tx pads have been proposed by researchers from Korea Advanced Institute of Science and Technology, such as I-type [10], S-type [11], and N-type [12]. Since the coupling coefficient is consistent against the displacement, there is no significant power fluctuation and only simple control designs are needed. However, the main drawback of the long-track scheme is the relatively low coupling coefficient, which degrades the power efficiency and leads to high electromagnetic exposure.

To enhance coupling coefficients and minimize electromagnetic exposure, researchers have explored segmented Tx pads in DWPT systems [13], [14], [15]. Inspired by stationary wireless power transfer magnetic couplers, this approach involves closely matching the sizes of Tx and Rx pads to optimize the coupling coefficient. In DWPT systems, segmented Tx pads are arranged sequentially to form a long Tx track, allowing the Rx pad to receive power as it moves across these pads. However, challenges arise when the Rx pad is positioned above the spacing zone between two adjacent Tx pads, resulting in weak magnetic coupling and subsequent power fluctuations. Studies have attempted to mitigate this issue by optimizing the physical size of the Tx pads, considering factors such as the coupling coefficient and the continuity of the Tx pads [9], [14]. To further reduce power fluctuations, some approaches eliminate spacing between Tx pads, as highlighted in Fig. 1(a), enhancing the magnetic fields in the spacing zone [16], [17], [18], [19]. For instance, Lu et al. [16] and Chen et al. [18] employed arrays of rectangular and double D quadrature pads (DDQPs), respectively, without spacing. An integrated design

Manuscript received 21 February 2024; revised 13 May 2024 and 12 June 2024; accepted 21 July 2024. Date of publication 23 July 2024; date of current version 4 September 2024. This work was supported in part by the National Natural Science Foundation of China under Grant 52007067, in part by the Science and Technology Planning Project of Guangdong Province under Grant 2023A0505050124, and in part by the Natural Science Foundation of Guangdong Province under Grant 2023A1515011623. Recommended for publication by Associate Editor J.-I. Itoh. *(Corresponding author: Zhicong Huang.)*

The authors are with the Shien-Ming Wu School of Intelligent Engineering, South China University of Technology, Guangzhou 510006, China (e-mail: zhiconghuang@scut.edu.cn).

Color versions of one or more figures in this article are available at https://doi.org/10.1109/TPEL.2024.3432815.

Digital Object Identifier 10.1109/TPEL.2024.3432815

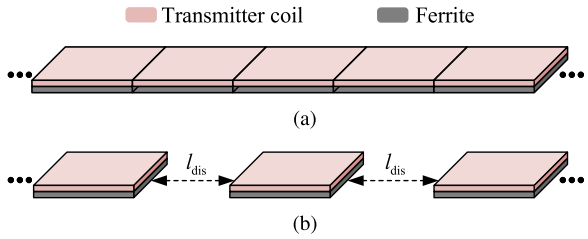

Fig. 1. Segmented transmitter layout model of DWPT system. (a) Without spacing distance. (b) With spacing distance.

method based on the continuous much longer Tx rectangular pads is proposed in Shi et al. [20] and [21] to suppress the power fluctuation in the DWPT system. However, this lack of spacing can result in significant cross-coupling between transmitter pads, necessitating complex parameter designs for compensation networks or additional mutual conductor designs [22]. It is crucial to note that these design methods may increase copper usage and core consumption due to the absence of array distance and continuous core design.

On the contrary, some researchers have explored alternative approaches by designing a segmented transmitter track with spacing between adjacent pads, as illustrated in Fig. 1(b), based on either unipolar or bipolar configurations. However, a common drawback of such designs, characterized by a large spacing distance, is the emergence of significant power fluctuation [23], [24], [25], [26]. For example, in the study by Lee et al. [24], the output power diminishes almost to zero when the receiver is located in the spacing zone. In addition, power pulsation reaching 50% occurs when the distance between adjacent transmitter pads is around 30% of the individual transmitter length in some DWPT systems [26]. To mitigate this power fluctuation, some solutions involve adopting a complex or larger pad on the receiver side. In a specific case, Zhao et al. [27] wounded solenoid coils around a long straight magnetic core plate to configure a bipolar-nonsalient pole transmitter. The receiver in this setup adopts two much larger cross-tiled DD coils. However, this results in a complex and cumbersome receiver side that demands more installation space, making it less practical for real-world applications [28], [29]. Another approach, detailed in [30], focuses on enhancing magnetic field concentration by employing solenoid coils with I-shaped cores to couple a large rectangular pad for a DWPT system. While this design achieves low power fluctuation, it compresses the height of the coupling magnetic field, leading to a reduced power transfer gap and significant practical limitations.

It is known that a unipolar–bipolar pad can generate (or capture) both vertical and horizontal magnetic fields in a complementary manner, thereby enhancing misalignment tolerance. As such, this hybrid transmitter pad presents a promising approach for constructing a segmented transmitter track in DWPT systems to mitigate power transfer fluctuation with a large spacing distance. However, owing to the hybrid magnetic field characteristics of this transmitter pad track, its matrix layout and driving method differ from traditional unipolar or bipolar transmitter tracks discussed earlier. These distinctions are notably absent in existing research and methodologies, warranting comprehensive exploration and analysis.

To address the aforementioned challenges, this article conducts an in-depth analysis of the magnetic flux characteristics and working principles associated with the mutual complementation mechanism of unipolar–bipolar pads. Subsequently, we propose an innovatively designed segmented transmitter track, featuring an alternately arranged arrangement of rectangular-solenoid pads (RSPs) for DWPT systems. The key novelties and contributions of this article are summarized as follows:

1) Novel transmitter track: We introduce a novel transmitter track based on the alternately arranged segmented RSPs. This transmitter track leverages magnetic field complementation to effectively mitigate output fluctuation on the receiver side, providing robust performance against a wide-range and dynamic displacement.
2) Large spacing distance design: The proposed alternately arranged segmented transmitter track allows for a considerable spacing distance between adjacent transmitter pads. This design choice not only facilitates a reduction in copper and ferrite core usage, but also addresses cross-coupling issues. Furthermore, it enables uniform sizing of the transmitter (Tx) and receiver (Rx) pads, maximizing the coupling coefficient for optimal power transfer capability relative to given copper usage and ferrite core constraints [31].
3) Orthogonal excitation method: We present a novel DWPT system incorporating an orthogonal excitation method tailored to the proposed alternately arranged segmented hybrid track. In addition, we provide a detailed methodology for parameter design, ensuring the system's effectiveness.

The rest of this article is organized as follows. Section II analyzes the working principle of the mutual complementation mechanism for RSP, and then proposes a alternately arranged segmented Tx track for DWPT systems. In Section III, a detailed excitation method of DWPT systems based on the proposed coupler is presented, along with the corresponding parameter design methodology. Section IV experimentally validates the proposed design and analysis. Finally, Section V concludes this article.

II. Proposed DWPT Track Based on Alternately Arranged Segmented RSPs

A. Characteristics of RSP

The RSP design has significant advantages over the conventional DDQP because it can achieve misalignment tolerance with less copper usage, which has been comprehensively demonstrated in our recently published work [32]. Taking this advantage in mind, the proposed DWPT track is based on segmented RSPs with an alternate arrangement. Fig. 2 depicts a single RSP that consists of a rectangular coil and a solenoid coil in the transmitter. The solenoid coil is wound around the core in an orthogonal layout with the rectangular coil. As a result, the coils on the Tx side are spatially integrated and magnetically decoupled. The rectangular coil produces a vertical magnetic field, while the solenoid coil generates a parallel magnetic field.

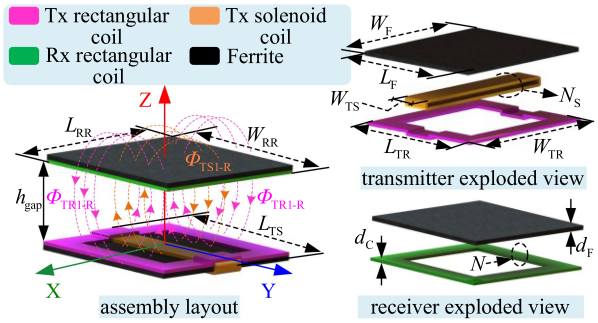

Fig. 2. Proposed single RSP.

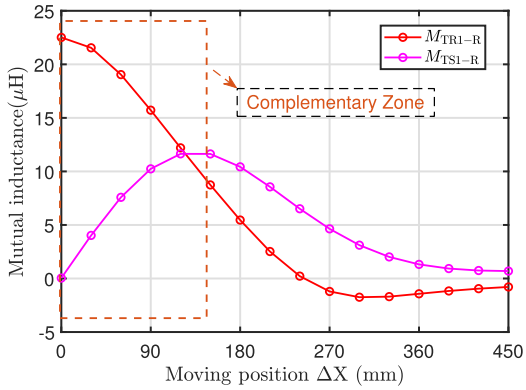

Fig. 3. Mutual inductance of RSP at various moving positions.

TABLE I
PARAMETERS OF THE COUPLER

Symbols	Parameters	Value (mm)
L_{RR}	Lenght of Rx rectangular coil	300
W_{RR}	Width of Rx rectangular coil	300
L_{TS}	Lenght of Tx solenoid coil	306
W_{TS}	Width of Tx solenoid coil	27
L_{TR}	Lenght of Tx rectangular coil	300
W_{TR}	Width of Tx rectangular coil	300
L_{F}, W_{F}, d_{F}	Ferrite dimensions	300,300,3
d_{C}	Litz wire diameter of coils	3
h_{gap}	Power transfer gap distance	100
N	Turn numbers of rectangular coils	10
N_{S}	Turn numbers of rectangular coils	9
P_{N}	Turn space of coils	0

On the Rx side, a rectangular coil is used to capture the magnetic flux generated by the RSP. The RSP on the Tx side and the rectangular coil on the Rx side form a three-winding loosely coupled transformer.

As highlighted in Fig. 2, the magnetic flux generated from Tx rectangular coil is donated as $\Phi_{\mathrm{TR1\text{-}R}}$, while the magnetic flux produced from the Tx solenoid coil is indicated as $\Phi_{\mathrm{TS1\text{-}R}}$. Both $\Phi_{\mathrm{TR1\text{-}R}}$ and $\Phi_{\mathrm{TS1\text{-}R}}$ represent the components of the magnetic flux in normal directions. Therefore, the mutual inductance between Tx rectangular pad and the Rx pad as well as that between Tx solenoid pad and the Rx pad can be, respectively, expressed as

$$M_{\mathrm{TS1\text{-}R}} = \frac{\Phi_{\mathrm{TS1\text{-}R}}}{I_{\mathrm{TS1}}}$$
$$M_{\mathrm{TS1\text{-}R}} = \frac{\Phi_{\mathrm{TS1\text{-}R}}}{I_{\mathrm{TS1}}}. \quad (1)$$

where I_{TR1} and I_{TS1} are the excitation current of the Tx rectangular coil and Tx solenoid coil, respectively.

Given the aforementioned analysis, the mutual inductance of a single RSP based on the parameters in Table I is plotted in Fig. 3. It can be observed that the $M_{\mathrm{TS1\text{-}R}}$ can be complementary with $M_{\mathrm{TR1\text{-}R}}$ in a certain range. Taking this advantage in mind, the RSPs can be designed for DWPT systems with an appropriate array and excitation approach, which will be put forward in detail as follows.

B. Alternately Arranged Segmented RSPs for DWPT

Based on the characteristics of the RSP, a DWPT Tx track consisting of alternately arranged RSPs is proposed as the front view shown in Fig. 4. The RSPs are arranged sequentially on the Tx side along the direction of movement, while the Rx side is designed with a simple rectangular pad, as illustrated in Fig. 4(a). l_{dis} is the spacing distance between the adjacent RSPs and set as 50% of the length of a single RSP, i.e., $l_{\mathrm{dis}} = 150$ mm. The spacing distance is significantly large and requires a specific arrangement as well as associate excitation to suppress power fluctuation across the spacing area.

All the rectangular coils in the Tx RSPs are wounded identically, generating unified vertical magnetic flux right above the RSPs as illustrated in Fig. 4(a). On the contrary, the solenoid coils are wounded alternately. The odd solenoid coils are wound in an anti clockwise direction, while the even ones are wound clockwise. Such that, the solenoid coils generate alternating horizontal magnetic flux across the RSPs. As illustrated in Fig. 4(b) (simulated results in ANSYS Maxwell), the magnetic cores of the RSPs exhibit a dual-pole pattern alternating between North–South (NS) and South–North (SN). Owing to the "NS–SN–NS–SN" arrangement, continuous magnetic paths are established, making the magnetic flux in the spacing areas vertical. Moreover, the magnetic flux magnitude in the spacing areas is consistent, but the direction alternates oppositely, e.g., the odd spacing area is downward, while the even spacing area is upward.

With the abovementioned design of the Tx track, the Rx RP can capture vertical magnetic flux right over the RSPs and in the spacing areas, which are generated by the Tx rectangular coils and solenoid coils, respectively. With the geometric specifications given in Table I, a finite element simulation is conducted to simulate the proposed DWPT track. As the Rx RP moves along the Tx track, the mutual inductances between the Rx RP and the individual Tx rectangular coils are shown in Fig. 5. Periodically, there exists a peak mutual inductance when the Rx RP is right over a Tx RSP. When the Rx RP misaligns with the Tx RSPs, the mutual inductances decrease sharply. Especially, there exists nearly null coupling in the spacing area. The overall rectangular-to-rectangular mutual inductance is given by

$$M_{\mathrm{TR\text{-}R}} = M_{\mathrm{TR1\text{-}R}} + M_{\mathrm{TR2\text{-}R}} + \cdots + M_{\mathrm{TR}i\text{-}\mathrm{R}} \quad (2)$$

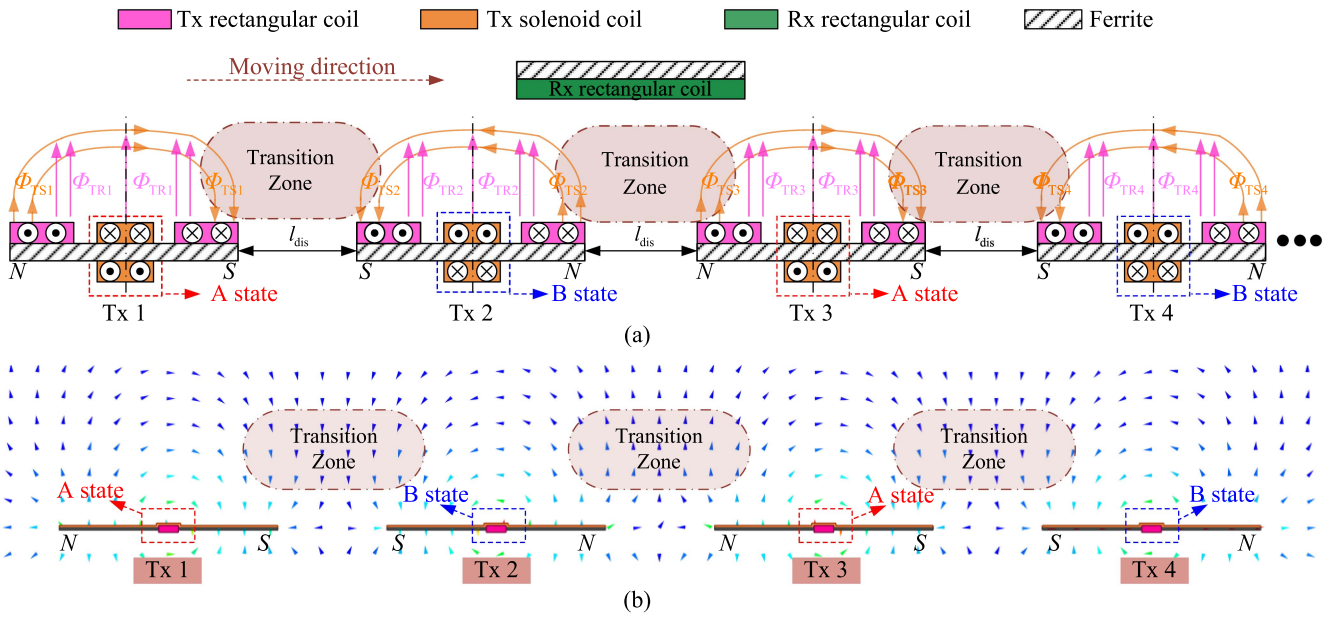

Fig. 4. Front view of the proposed DWPT Tx track consisting of alternately-arranged RSPs. Unless specified, subscripts TR, TS, and R are used to indicate parameters of the Tx rectangular coil, Tx solenoid coil, and Rx rectangular coil, while $i = 1, 2, 3$, etc. represents associated the Tx RSP order.

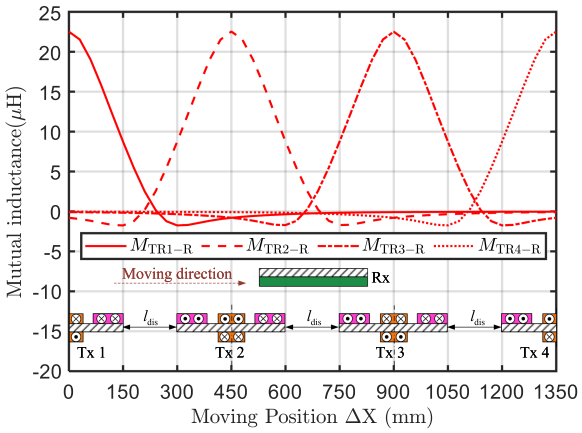

Fig. 5. Mutual inductances between the Rx RP and the individual Tx rectangular coils.

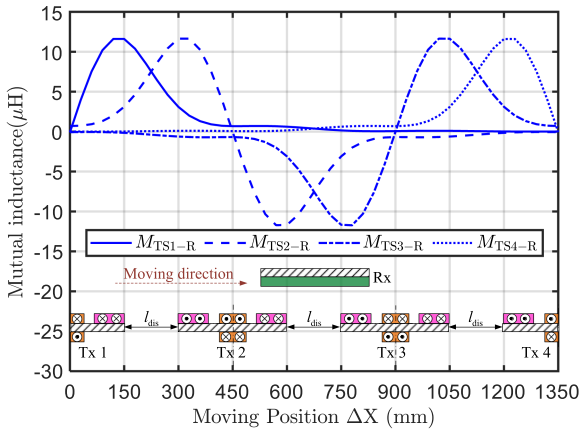

Fig. 6. Mutual inductances between the Rx RP and the individual Tx solenoid coils.

and it is plotted as the red solid curve in Fig. 7. Similarly, the mutual inductances between the Rx RP and the individual Tx solenoid coils are shown in Fig. 5. When the Rx RP is positioned within the spacing areas, it establishes mutual coupling with the adjacent solenoid coils. It can enable power delivery even when the Rx RP experiences a significant offset with the Tx RSPs. The overall solenoid-to-rectangular inductance is given by

$$M_{\text{TS-R}} = M_{\text{TS1-R}} + M_{\text{TS2-R}} + \cdots + M_{\text{TS}i\text{-R}} \tag{3}$$

and it is plotted as the blue dashed curve in Fig. 7.

From Fig. 7, mutual coupling consistently exists as the Rx RP moves along the whole Tx track, but the situations are alternating in the spacing areas. In the odd spacing areas, $M_{\text{TR-R}}$ and $M_{\text{TS-R}}$ are both positive and their slopes have a complementary tendency with the position change. However, in the even spacing

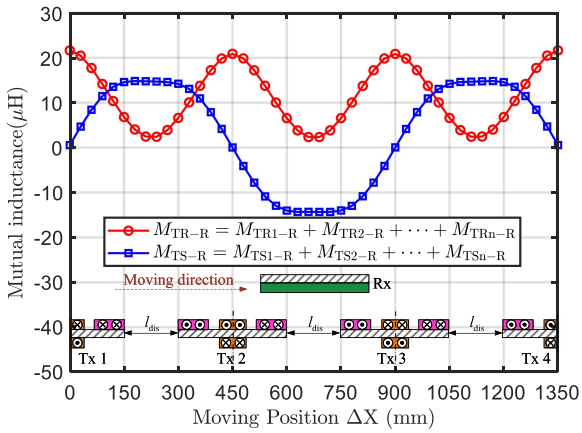

Fig. 7. Overall rectangular-to-rectangular and solenoid-to-rectangular mutual inductances.

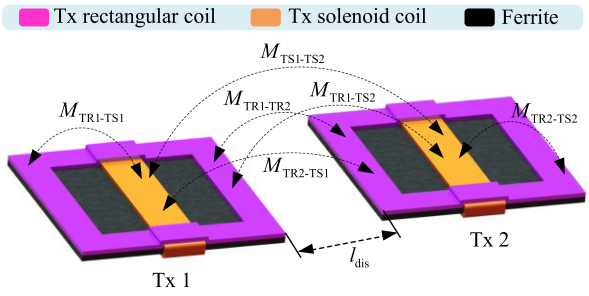

Fig. 8. Definition of cross-coupling between the adjacent RSP.

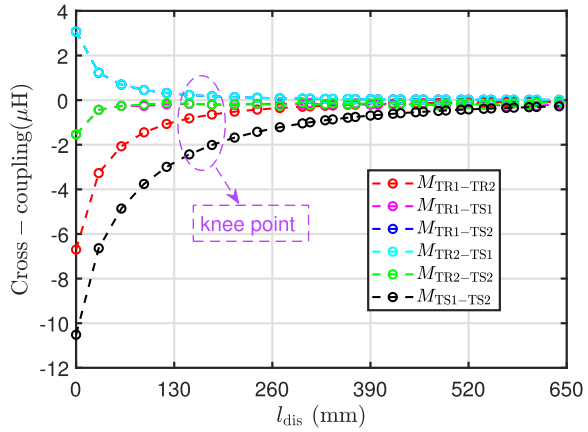

Fig. 9. Cross-coupling between the adjacent RSP versus l_{dis}.

areas, $M_{\mathrm{TR\text{-}R}}$ remains positive and axially symmetric to that in the adjacent spacing areas, but $M_{\mathrm{TS\text{-}R}}$ is negative and centrally symmetric to that in the adjacent spacing areas. A straightforward way to tackle the abovementioned issue is by detecting the zero-crossing of $M_{\mathrm{TS\text{-}R}}$ and using active control strategies. Such a scheme increases complexity and decreases robustness, making it less feasible in a practical DWPT system with many Tx RSPs. In Section III, a purely passive way without complex detection and active control will be developed to achieve stable output.

C. Cross-Coupling Issue and Spacing Distance Design

To mitigate circulating current, it is essential to minimize the cross-coupling between segmented Tx RSPs. While increasing the spacing distance l_{dis} between Tx RSPs can help reduce cross-coupling, it exacerbates power fluctuation. Therefore, a careful design is necessary. The major cross-coupling between the coils of the adjacent RSPs is highlighted in Fig. 8. According to the FEA results, the mutual inductances represented as per-unit values are shown in Fig. 9. The base value is the mutual inductance in the fully aligned condition, given by $M_{\mathrm{TR\text{-}R}}|_{\mathrm{aligned}} = 22.52\,\mu\mathrm{H}$. There is a significant initial decrease in the mutual inductances and the reduction becomes less pronounced as l_{dis} continues to increase until it reaches 150 mm, where the mutual inductances converge to zero. The maximum mutual inductance attributed

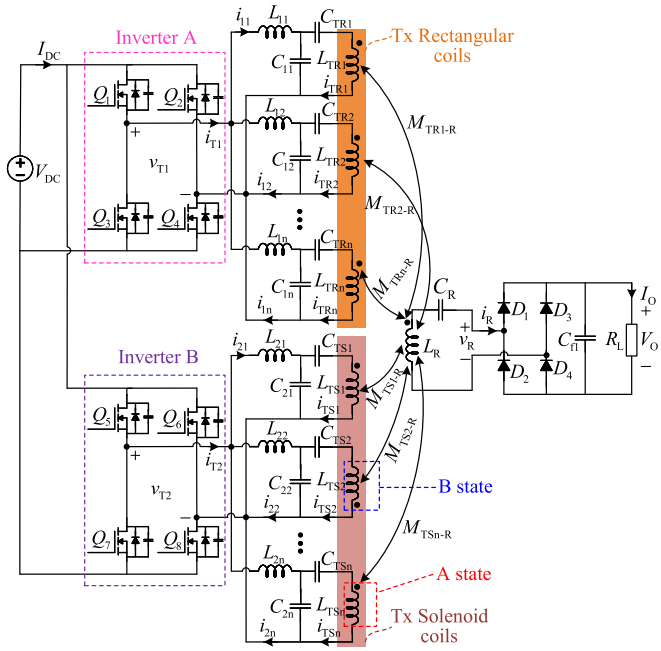

Fig. 10. Circuit configuration of proposed DWPT system.

to the cross-coupling issue constitutes only a small percentage (8.2%) of that utilized for power transfer. To simplify the circuit analysis, they are ignored in the subsequent sections. Without loss of generality, the spacing distance is set at 150 mm.

III. Proposed DWPT System

A. System Schematics

The schematics of the proposed DWPT system are shown in Fig. 10. The Tx track includes n RSPs with alternating arrangement as proposed in Section II. All Tx coils are compensated by *LCC* circuits, while the single Rx coil is series compensated. Thus, the weight and complexity of the Rx side can be reduced and simplified significantly.

The Tx track is driven by two individual inverters. The MOSFETs Q_1–Q_4 constitute a full-bridge inverter A to make input dc voltage V_{DC} into high-frequency square wave voltage v_{T1}, which will feed the Tx rectangular coils through the corresponding *LCC* compensation network. Another full-bridge inverter B composed of the MOSFETs Q_5–Q_8 is developed to output a high-frequency square wave voltage v_{T2} to supply the Tx solenoid coils with the help of its *LCC* compensation network. These two inverters are connected in parallel to share a single dc source and operate independently. All the Tx rectangular coils are in parallel and driven by inverter A, while similarly all the solenoid coils are driven by inverter B. On the Rx side, diodes D_1–D_4 form a passive full-bridge rectifier to rectify the induced ac output voltage of the Rx rectangular coil. V_{O} and I_{O} are the output voltage and output current, respectively. The equivalent load resistance of the DWPT system is donated as $R_L = \frac{V_{\mathrm{O}}}{I_{\mathrm{O}}}$. Circuit parameters of the proposed DWPT system is summarized in Table II.

TABLE II
DESCRIPTION OF CIRCUIT PARAMETERS

Symbols	Descriptions
$L_{\mathrm{TR}i}$ $(i=1,2,...,n)$	Self-inductances of Tx rectangular coils
$L_{\mathrm{TS}i}$ $(i=1,2,...,n)$	Self-inductances of Tx solenoid coils
L_{1i}, C_{1i}, $C_{\mathrm{TR}i}$ $(i=1,2,...,n)$	Compensation inductors and capacitors of *LCC* network for Tx rectangular coils
L_{2i}, C_{2i}, $C_{\mathrm{TS}i}$ $(i=1,2,...,n)$	Compensation inductors and capacitors of *LCC* network for Tx solenoid coils
L_{R} and C_{R}	Self-inductance of Rx rectangular coil and corresponding series compensation capacitor
$M_{\mathrm{TR}i\text{-R}}$ (or $M_{\mathrm{TS}i\text{-R}}$) $(i=1,2,...,n)$	Mutual inductances between Tx rectangular (or solenoid) coils and Rx rectangular coil
$i_{\mathrm{TR}i}$ (or $i_{\mathrm{TS}i}$) $(i=1,2,...,n)$	Driving currents of Tx rectangular (or solenoid) coils
i_{1i} (or i_{2i}) $(i=1,2,...,n)$	Input currents of *LCC* networks for Tx rectangular (or solenoid) coils
i_{T1} and i_{T2}, i_{R}	Output current of inverters A and B respectively, input currents of Rx rectifier

B. Modeling and Analysis of the Proposed DWPT System

As highlighted in Fig. 10, the inverters A and B on Tx side operate independently, thus taking the ac voltage v_{T1} as a reference, the phase difference between v_{T1} and v_{T2} is defined as θ. Fundamental approximation method is used for subsequent analysis. Without loss of generality, $\boldsymbol{V}_{\mathrm{T1}}$, $\boldsymbol{V}_{\mathrm{T2}}$, $\boldsymbol{I}_{1\mathrm{i}}$, $\boldsymbol{I}_{2\mathrm{i}}$, $\boldsymbol{I}_{\mathrm{TRi}}$, $\boldsymbol{I}_{\mathrm{TSi}}$, and $\boldsymbol{I}_{\mathrm{R}}$ are corresponding fundamental vectors of v_{T1}, v_{T2}, $i_{1\mathrm{i}}$, $i_{2\mathrm{i}}$, i_{TRi}, i_{TSi}, and i_{R}, respectively. The output voltages of the inverters can be expressed as

$$\begin{aligned}\boldsymbol{V}_{\mathrm{T1}} &= \frac{4}{\pi} V_{\mathrm{DC}} \angle 0^{\circ} \\ \boldsymbol{V}_{\mathrm{T2}} &= \frac{4}{\pi} V_{\mathrm{DC}} \angle \theta^{\circ}.\end{aligned} \tag{4}$$

The compensation components L_{1i}, C_{1i}, L_{2i}, and C_{2i} in the Tx RSPs together with the series resonant circuit (L_{R}, C_{R}) on the Rx side are designed to be fully resonant, i.e., $\omega = 1/\sqrt{L_{1i}C_{1i}} = 1/\sqrt{L_{1i}C_{1i}} = 1/\sqrt{L_{\mathrm{R}}C_{\mathrm{R}}}$ $(i = 1, 2, 3, \ldots, n)$. All the compensation conductors and corresponding capacitors of *LCC* networks for $L_{\mathrm{TR}i}$ are identically designed, i.e., $L_{1i} = L_1$, $C_{1i} = C_1$, and $C_{\mathrm{TR}i} = C_{\mathrm{TR}}$. Similar designs are also applied to $L_{\mathrm{TS}i}$ are the same, i.e., $L_{2i} = L_2$, $C_{2i} = C_2$, and $C_{\mathrm{TS}i} = C_{\mathrm{TS}}$. The parasitic resistances of the coils and the compensation components are ignored to simplify the analysis. Based on the well-known analysis of *LCL* circuits [16], [22], [25], [33], [34], the DWPT system is driven by two current sources, and the output voltage $\boldsymbol{V}_{\mathrm{R}}$ can be readily derived as

$$\boldsymbol{V}_{\mathrm{R}} = \omega^2 C_1 \sum_{i=1}^{n} M_{\mathrm{TR}i\text{-R}} \boldsymbol{V}_{\mathrm{T1}} + \omega^2 C_2 \sum_{i=1}^{n} M_{\mathrm{TS}i\text{-R}} \boldsymbol{V}_{\mathrm{T2}}. \tag{5}$$

Subsequently, with (4), (5), and following the trigonometric law of cosines, the dc output voltage of the proposed DWPT systems can be described as follows:

$$V_{\mathrm{O}} = \frac{\pi}{4} |\boldsymbol{V}_{\mathrm{R}}| = \omega^2 V_{\mathrm{DC}} C_1 \sqrt{\alpha + \beta} \tag{6}$$

where

$$\alpha = \left(\sum_{i=1}^{n} M_{\mathrm{TR}i\text{-R}} \right)^2 + \frac{C_2^2}{C_1^2} \left(\sum_{i=1}^{n} M_{\mathrm{TS}i\text{-R}} \right)^2 \tag{7}$$

$$\beta = \frac{2C_2 \sum_{i=1}^{n} M_{\mathrm{TR}i\text{-R}} \sum_{i=1}^{n} M_{\mathrm{TS}i\text{-R}} \cos\theta}{C_1}. \tag{8}$$

With (6), it is evident that the dc output voltage V_{O} is related to $M_{\mathrm{TR\text{-}R}}$ (i.e., $\sum_{i=1}^{n} M_{\mathrm{TR}i\text{-R}}$) and $M_{\mathrm{TS\text{-}R}}$ (i.e., $\sum_{i=1}^{n} M_{\mathrm{TS}i\text{-R}}$). There are two different terms and thus the basic idea to suppress power fluctuation for the proposed DWPT system based on complementary of $M_{\mathrm{TR\text{-}R}}$ and $M_{\mathrm{TS\text{-}R}}$ can be obtained as follows.

1) Term β is relevant to the polarity of $M_{\mathrm{TR\text{-}R}}$ and $M_{\mathrm{TS\text{-}R}}$. As illustrated in Section II, $M_{\mathrm{TS\text{-}R}}$ exhibits zero-crossing polarity reversal, causing term β to encounter the same issue. Therefore, there are two main schemes to operate the proposed DWPT system independent of the polarity of $M_{\mathrm{TR\text{-}R}}$ and $M_{\mathrm{TS\text{-}R}}$. First, polarity detection of $M_{\mathrm{TS\text{-}R}}$ and reverse shifting of θ is an active way to address this issue, but the detection and control are complex. Alternatively, to fully eliminate the control effort, β can be nullified by setting θ to be $\pi/2$ in this article.
2) Term α is regardless to the polarity of $M_{\mathrm{TR\text{-}R}}$ and $M_{\mathrm{TS\text{-}R}}$. Since the changes of $M_{\mathrm{TR\text{-}R}}^2$ and $M_{\mathrm{TS\text{-}R}}^2$ are complementary to each other during the moving process of Rx RP, Such that, it is possible to construct a nearly constant α in the whole moving direction by designing C_1 and C_2.

Once the design of term α and term β are satisfied, the proposed DWPT system can operate irrelevant to the polarity of $M_{\mathrm{TR\text{-}R}}$ and $M_{\mathrm{TS\text{-}R}}$ and achieve suppressing power fluctuation based on the magnetic field complementary without the necessity of complex detection and active control. Based on the abovementioned, when $\theta = \pi/2$, Term β is zero, and the V_{O} can be rewritten as

$$V_{\mathrm{O}} = \omega^2 V_{\mathrm{DC}} C_1 \sqrt{\alpha}. \tag{9}$$

From (9), the output voltage is load-independent and a CV output can be expected. It is configurable by tuning the compensation parameter C_1 and not restricted by the magnetic coupler.

C. Parameters Design for Power Fluctuation Suppression

Based on (9), the fluctuation of output voltage V_{O} is determined by α given as

$$\alpha = M_{\mathrm{TR\text{-}R}}^2 + \lambda M_{\mathrm{TS\text{-}R}}^2 \tag{10}$$

where

$$\lambda = \frac{C_2^2}{C_1^2}. \tag{11}$$

As highlighted in (10), the mutual inductance $M_{\mathrm{TR\text{-}R}}$, $M_{\mathrm{TS\text{-}R}}$, and λ are affect factors in fluctuation of the output voltage. Thus, a straightforward approach is to adjust the $M_{\mathrm{TR\text{-}R}}$ and $M_{\mathrm{TS\text{-}R}}$ based on the parameters design of the Tx RSP for achieving a stable output characteristic during the moving process. This way will restrict coupler design freedom significantly as well as be time-consuming. As illustrated in Fig. 7, the absolute value

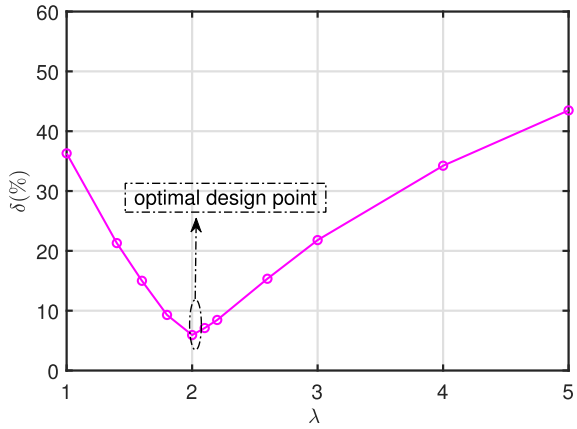

Fig. 11. Fluctuation value δ versus λ.

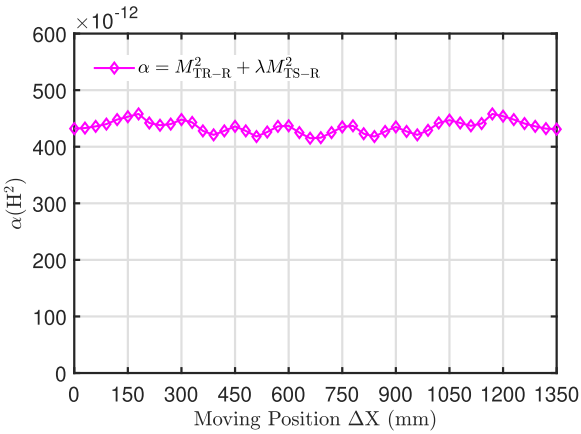

Fig. 12. α versus displacement.

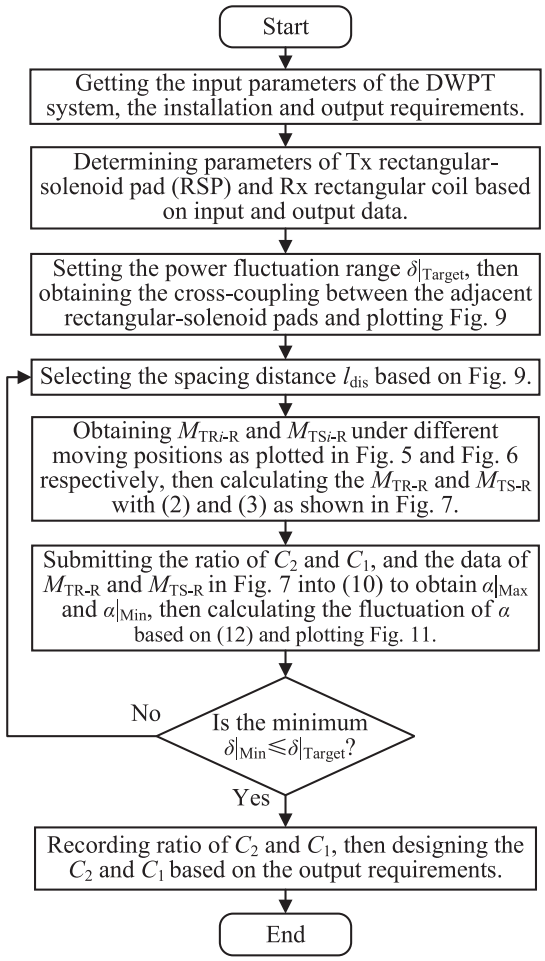

Fig. 13. Design flowchart for the proposed DWPT system.

of mutual inductance $M_{\text{TR-R}}$ and $M_{\text{TS-R}}$ have opposite trends and in a complementary manner during the moving process. Such that, with (10), it is evident that α can be designed to be a relatively stable value versus moving positions via selecting an appropriate λ. In other words, the variation of the output voltage V_{O} can be suppressed, along with unleashing the design freedom in RSP. The fluctuation of the α is defined as

$$\delta = \frac{\alpha|_{\text{Max}} - \alpha|_{\text{Min}}}{\alpha|_{\text{Max}} + \alpha|_{\text{Min}}} \times 100\%. \tag{12}$$

Here, $\alpha|_{\text{Max}}$ and $\alpha|_{\text{Min}}$ are the maximum and minimum values of α versus the moving positions.

According to (12) and mutual inductance shown in Fig. 7, the fluctuation value δ with various λ are plotted in Fig. 11. It can be advised that δ first decreases and then increases as a rise of λ. Thus, the minimum point represents the most advantageous design point with minimal fluctuations, as shown in Fig. 11. To be specific, with the design given in Fig. 11 as well as $M_{\text{TR-R}}$ and $M_{\text{TS-R}}$ in Fig. 7, α can be calculated according to (10). Thus, α versus misalignment can be plotted as shown in Fig. 12. It can be observed that α is nearly constant and the fluctuation is within 5.1%. Such that, based on (9), a nearly constant V_{O} can be maintained over a wide-range displacement. Given the aforementioned analysis, a design flowchart to detail the design procedure and consideration for the proposed DWPT system is shown in Fig. 13. The design procedure of the proposed DWPT system can be summarized as follows.

1) Getting the input parameters and the output requirements of the proposed DWPT system, such as the input dc voltage, input power, operating frequency, the output voltage, and output rated power, etc. Then, determining the parameters of the Tx rectangular and solenoid coils, and the Rx rectangular coil according to the input and output data.
2) Setting the power fluctuation range δ_{Target} and obtaining the cross-coupling between the adjacent RSPs and plotting Fig. 9. Then selecting the spacing distance l_{dis} based on Fig. 9.
3) Obtaining the mutual inductances $M_{\text{TR}i\text{-R}}$ and $M_{\text{TS}i\text{-R}}$ under different moving positions as plotted in Figs. 5 and 6, respectively. Then calculating the $M_{\text{TR-R}}$ and $M_{\text{TS-R}}$ based on (2) and (3) as shown in Fig. 7. Afterward, submitting the ratio of C_2 and C_1, as well as the data of the $M_{\text{TR-R}}$ and $M_{\text{TS-R}}$ in Fig. 7 into the (10) to obtain the $\alpha|_{\text{Max}}$ and $\alpha|_{\text{Min}}$. Finally, submitting $\alpha|_{\text{Max}}$ and $\alpha|_{\text{Min}}$ into (12) to calculate the fluctuation of the α and plotting Fig. 11.

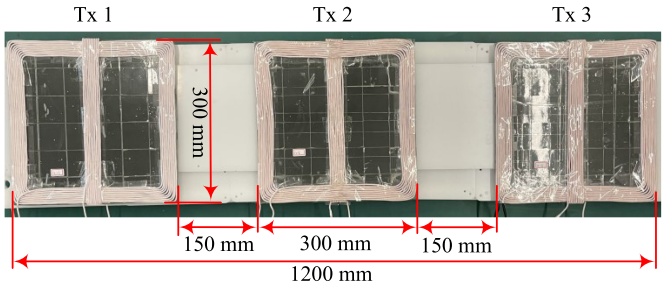

Fig. 14. Practical structure and dimension of proposed DWPT transmitter.

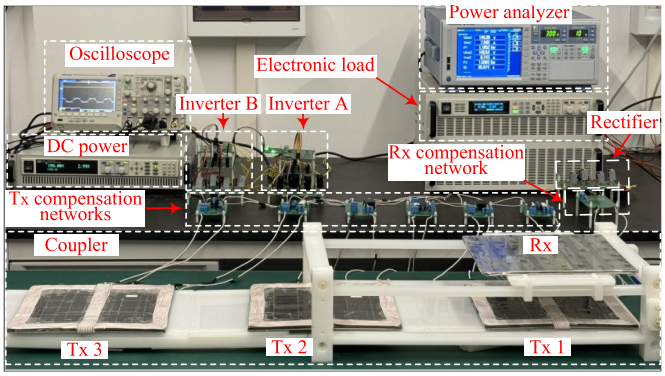

Fig. 15. Experimental prototype of 1 kW proposed DWPT system with alternately-arranged segmented transmitters.

4) When the fluctuation $\delta_{\mathrm{Min}} \leq \delta_{\mathrm{Target}}$ achieves, the corresponding ratio value of C_2 and C_1 is the optimal design point for the proposed DWPT system to achieve the best power fluctuation suppression capability during the moving profile. Thus, recording this ratio of C_2 and C_1 and designing C_2 and C_1 based on the output requirements. However, if the $\delta_{\mathrm{Min}} > \delta_{\mathrm{Target}}$, the spacing distance l_{dis} should be reselected according to Fig. 9 and redesigned.

IV. Experimental Verification

A. Experiment Setup

To verify the design and analysis of the proposed DWPT systems, a three-module scale-down 1 kW DWPT system laboratory prototype operating at 85 kHz switching frequency is built based on the schematic in Fig. 10, as depicted in Fig. 15. The proposed DWPT coupler, as illustrated in Fig. 14, is manufactured based on the configuration in Fig. 4 with the parameters provided in Section II. The dc input voltage V_{DC} is fixed at 150 V, consequently, with the one-to-one voltage gain design, the required output voltage is also 150 V. A *LCR* meter HIOKI IM3536 is utilized to measure the self-inductances (L_{TRi}, L_{TSi}, and L_{R}) and the compensation parameters are designed based on Section III, which are detailed in Table III. The STC4050 MOSFETs Q_1–Q_8 are selected while the Rx rectifier (D_1–D_4) uses diodes MBR20200CTG. The two inverters (i.e., inverters A and B) share a digital controller. The controller generates two groups of PWM signals to drive the two independent inverters. The phase difference between these two group PWMs is set to be 90°, such that it can achieve a phase difference of 90° between the two independent inverters. A programmable dc electronic load (DH27605B) is employed to simulate a battery load, while the power analyzer YOKOGAWA WT1803E is used to measure the power distribution and the overall dc–dc efficiency of the proposed system.

TABLE III
Measured Parameters of the DWPT Prototype

Coupler parameters		Circuit parameters	
Symbols	Value	Symbols	Value
$L_{\mathrm{TR}i}$ (i=1,2,3)	99.82 μH, 99.56 μH, 99.21 μH	L_1, L_2	21.65 μH, 15.32 μH
$L_{\mathrm{TS}i}$ (i=1,2,3)	101.81 μH, 100.98 μH, 101.36 μH	C_1, C_2	161.9 nF, 228.95 nF
L_{R}	99.86 μH	C_{R}	35.18 nF
h_{gap}	100 mm	C_{TR},C_{TS}	41.96 nF, 42.06 nF
N	10	V_{DC}	150 V
N_{S}	9	D_1 -D_4	MBR20200CTG
d_{C}	3 mm	Q_1 -Q_8	STC 4050

B. Static Characteristics and Load-Independent Output Performance

Fig. 16(a) and (b) shows experimental waveforms of modulated voltage v_{T1}, input current i_{T1}, modulated voltage v_{T2}, input current i_{T2}, induced voltage v_{R}, induced current i_{R}, and output voltage V_{O} at different moving positions $\Delta\mathrm{X} =$ 0 mm and $\Delta\mathrm{X} = 675$ mm for full load with $R_{\mathrm{L}} = 22.5\,\Omega$, where $\Delta\mathrm{X} = 0$ mm is the position that the receiver is fully aligned with the Tx1 and $\Delta\mathrm{X} = 675$ mm indicates the position that the receiver arrives at the midpoint of the Tx2 and Tx3. It can be observed that the output voltage remains almost 150 V although the receiver moves to different positions. To validate the load-independent constant voltage (CV) output characteristic of the proposed DWPT system, an experimental process to step load from 20 Ω - 40 Ω - 80 Ω is implemented, as shown in Fig. 17. It can be observed that as the load R_{L} increases, the output current I_{O} decreases, while the output voltage V_{O} remains almost constant. Therefore, the proposed DWPT system possesses a good CV output property.

C. Dynamic Performance

To evaluate the system's performance while the receiver pad moves across the entire section (i.e., moving position $\Delta\mathrm{X}$ changes from 0 to 900 mm while $\Delta\mathrm{Y} = 0$ mm), dynamic experiments are carried out for the full load $R_{\mathrm{L}} = 22.5\,\Omega$ and half load $R_{\mathrm{L}} = 45\,\Omega$, as shown in Fig. 18(a) and (b), respectively. From Fig. 18, it is obvious that the output voltage V_{O} at full load and half load are consistent and almost constant during the moving profile. Fig. 20 provides the detailed V_{O} at full load for different moving positions along the moving direction. It should be noted that the fluctuation of the output voltage in the moving range $\Delta\mathrm{X} \in [0\,\mathrm{mm}\ 900\,\mathrm{mm}]$ is within $\pm 5.42\%$. Thus the proposed DWPT system possesses excellent power fluctuation suppression performance.

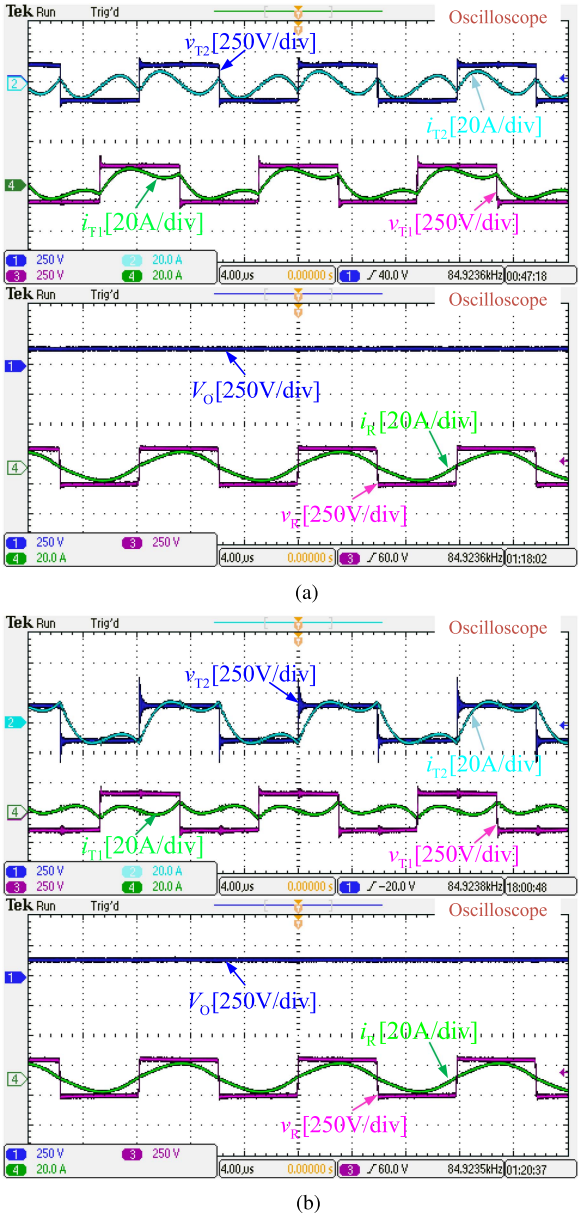

Fig. 16. Experimental waveforms of the proposed DWPT system at different moving positions. (a) $\Delta X = 0$ mm. (b) $\Delta X = 675$ mm.

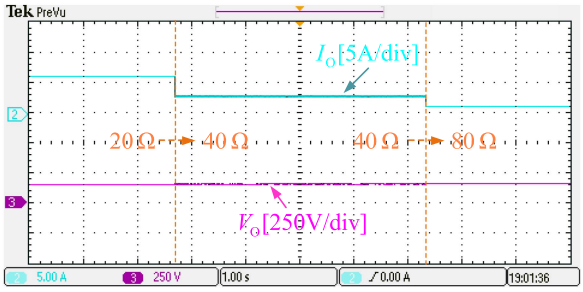

Fig. 17. Output currents and voltages at different load conditions.

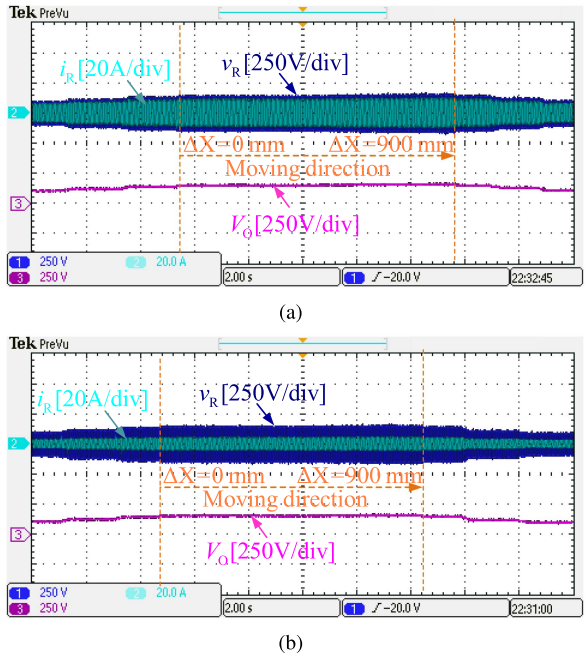

Fig. 18. Dynamic output currents and voltages at different load conditions. (a) full load $R_L = 22.5\,\Omega$ and (b) half load $R_L = 45\,\Omega$.

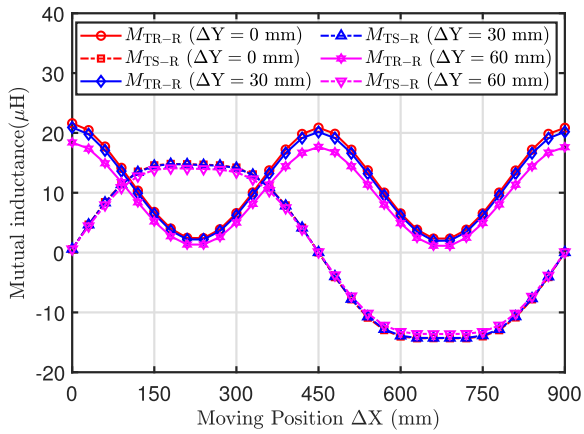

Fig. 19. Measured mutual inductance of the proposed DWPT system under different Y-axis (left or right) misalignment conditions during moving range $\Delta X \in$ [0 mm 900 mm].

The complementary characteristic of the magnetic field for suppressing output power fluctuation is always existing along the X-axis, and thus the Y-axis (left or right) misalignment will not affect the suppression of output power fluctuation over the wide-range displacement along the X-axis. The Y-axis (left or right) misalignment only affects the overall coupling coefficient. It can be validated by Fig. 19. When there is Y-axis misalignment as shown in Fig. 19, the relationship of $M_{\text{TR-R}}$ and $M_{\text{TS-R}}$ over the X-axis displacement is kept consistent. With the mutual inductances shown in Fig. 19, the output voltage can measured and plotted in Fig. 20. It can be observed that, when there is Y-axis misalignment, suppression of output fluctuation (also within 5.42%) against X-axis displacement can still be achieved.

TABLE IV
COMPARISONS WITH STATE-OF-THE-ART WORKS

Works	Tx & Rx Pad Structure	Tx & Rx Pad Size (cm)	Uniform Tx & Rx Pad Size	Spacing Distance / Tx Pad Size	Cost Due to Copper and Ferrite Usage	Output Fluctuation	Efficiency Fluctuation
[16]	RP & RP	38.8×40 & 48.5×40	No	0%	High	$\leq 7.5\%$	2.9%
[18]	DDQP & DDP	119×65 & 42×38	No	0%	High	$\leq 10.0\%$	4%
[19]	DDP+RP & DDQP	40×40 & 20×40	No	0%	High	$\leq 2\%$	2.3%
[21]	Anti-series RP & RP	90×45 & 40×40	No	3.3%	High	$\leq 4\%$	2.6%
[25]	DDP & DDP+QP	30×45 & 30×45	Yes	23.3%	low	54.8%	19%
[27]	SP & 2 cross-tiled DDP	55×10 & 150×80	No	9.1%	low	$\leq 36.7\%$	2.0%
This work	RSP & RP	30×30 & 30×30	Yes	50%	low	$\leq 5.42\%$	1.2%

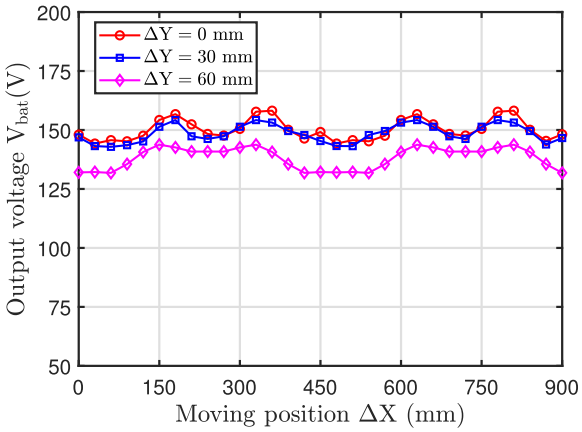

Fig. 20. Output voltage V_O at full load during moving range $\Delta X \in$ [0 mm 900 mm] at different Y-axis misalignment conditions.

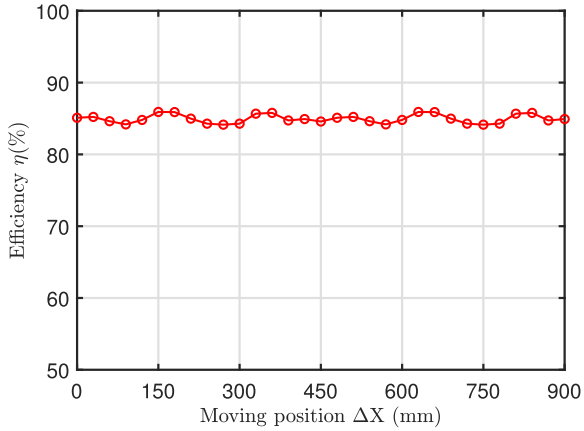

Fig. 22. Measured DC–DC efficiency of proposed DWPT system within moving range $\Delta X \in$ [0 mm 900 mm] at full load.

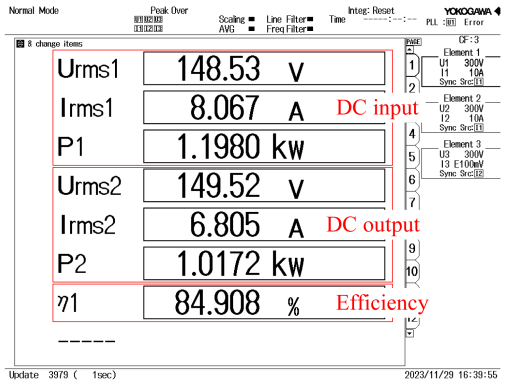

Fig. 21. Measured input and output characteristics of proposed DWPT system at middle position $\Delta X = 450$ mm for full load.

The amplitude of the output voltage decreases with the increase of Y-axis misalignment due to the decrease of overall coupling.

Fig. 21 illustrates the power efficiency measured by a power analyzer YOKOGAWA WT1803E (the Rx pad locates at $\Delta X = 450$ mm and $\Delta Y = 0$ mm, and the load condition is full). The output power and power transfer efficiency are 1.02 kW and 84.9%, respectively. The measured efficiency over the dynamic displacement is shown in Fig. 22, it can be observed that the efficiency ranges from 84.7% to 85.9%, which means there is only 1.2% fluctuation over the whole displacement range.

D. Comparison and Discussion

In order to suppress the power fluctuation and efficiency fluctuation in DWPT systems over wide-range displacement, some works have designed the segmented Tx track without spacing distance or with a very small spacing distance between the adjacent Tx pads, such as [16], [18], [19], and [21]. However, although these design methods can achieve power fluctuation suppression during the dynamic displacement, the adjacent transmitters suffer from significant cross-coupling, such that complex compensation designs or additional controls are required to address this issue. Moreover, it increases copper and ferrite usage due to continuous arrangement of the transmitter pad. Alternatively, some works design a segmented transmitter track with spacing between adjacent pads, such as [25] and [27]. Although this design can significantly alleviate cross-coupling and reduce copper and ferrite usage, a common issue is the

significant power fluctuation in the spacing zone. Therefore, there is still a research gap to suppress output fluctuation over wide-range dynamic displacement while allowing large spacing distance between transmitter pads and using passive approach without complex sensing and control.

This article aims to bridge the research gap and propose a novel transmitter track that can suppress output power fluctuation against the wide-range dynamic displacement. The structure is based on alternately arranged segmented RSPs, which has not yet been reported in the literature. A comparison is made between the performance of the proposed method and some existing methods as highlighted in Table IV. It can be observed that, significant advantages of the proposed design include wide spacing distance between the adjacent transmitter pads and allowing uniform size for the Tx and Rx pads to maximize coupling coefficient. The output fluctuation is within 5.42% when the spacing distance between the adjacent Tx pads is set to 150 mm (about 50% of the proposed RSP length). The fluctuation of the power efficiency is only 1.2%. Moreover, the proposed design utilizes a uniform Tx and Rx pad size, such that it can maximize the coupling coefficient for optimal power transfer capability compared with asymmetric Tx and Rx pad size [16], [18], [19], [21].

V. Conclusion

In this article, a novel transmitter track is proposed, which is based on alternately arranged segmented RSPs. The Tx track features magnetic field complementation to suppress the fluctuation of output on the receiver side against the wide-range and dynamic displacement, which are introduced and analyzed comprehensively. In addition, a novel DWPT system based on the proposed Tx track is developed with an orthogonal excitation method and a detailed parameter design methodology. A 1 kW DWPT experimental prototype using the proposed coupler and excitation method with a *LCC*-S topology is constructed to verify the analytical findings and design, and the experimental results show that the output voltage fluctuation is within 5.42% during the whole moving positions.

References

[1] M. Wilson, "Feasibility study: Powering electric vehicles on englands major roads," Bedford, U.K.: Highways England, Jul. 2015.

[2] D. Magnor, J. B. Gerschler, M. Ecker, P. Merk, and D. U. Sauer, "Concept of a battery aging model for lithium-ion batteries considering the lifetime dependency on the operation strategy," in *Proc. Eur. Photovolt. Sol. Energy Conf.*, 2009, pp. 21–25.

[3] V. Prasanth and P. Bauer, "Distributed IPT systems for dynamic powering misalignment analysis," *IEEE Trans. Ind. Electron.*, vol. 61, no. 11, pp. 6013–6021, Nov. 2014.

[4] V. B. Vu, M. Dahidah, V. Pickert, and V. T. Phan, "A high-power multiphase wireless dynamic charging system with low output power pulsation for electric vehicles," *IEEE J. Emerg. Sel. Topics Power Electron.*, vol. 8, no. 4, pp. 3592–3608, Dec. 2020.

[5] W. Zhang, S. C. Wong, C. K. Tse, and Q. Chen, "An optimized track length in roadway wireless power transfer systems," *IEEE J. Emerg. Sel. Topics Power Electron.*, vol. 2, no. 3, pp. 598–608, Sep. 2014.

[6] X. Li, J. Hu, H. Wang, X. Dai, and Y. Sun, "A new coupling structure and position detection method for segmented control dynamic wireless power transfer systems," *IEEE Trans. Power Electron.*, vol. 35, no. 7, pp. 6741–6745, Jul. 2020.

[7] Z. Deng et al., "Design of a 60kW EV dynamic wireless power transfer system with dual transmitters and dual receivers," *IEEE J. Emerg. Sel. Topics Power Electron.*, vol. 12, no. 1, pp. 316–327, Feb. 2024, doi: 10.1109/JESTPE.2023.3301579.

[8] Y. Geng, Q. Guo, Z. Yang, F. Lin, and Y. Wang, "Design and optimization of real-time strong coupling coil of dynamic wireless power transfer for electrical vehicle," *IEEE Trans. Veh. Technol.*, vol. 72, no. 9, pp. 11495–11504, Sep. 2023.

[9] R. Tavakoli, E. M. Dede, C. Chou, and Z. Pantic, "Cost-efficiency optimization of ground assemblies for dynamic wireless charging of electric vehicles," *IEEE Trans. Transport. Electrific.*, vol. 8, no. 1, pp. 734–751, Mar. 2022.

[10] J. Huh, S. W. Lee, W. Y. Lee, G. H. Cho, and C. T. Rim, "Narrow-width wireless power transfer system for online electrical vehicles," *IEEE Trans. Power Electron.*, vol. 26, no. 12, pp. 3666–3679, Dec. 2011.

[11] S. Y. Choi, S. Y. Jeong, B. W. Gu, G. C. Lim, and C. T. Rim, "Ultraslim S-type power supply rails for roadway-powered electric vehicles," *IEEE Trans. Power Electron.*, vol. 30, no. 11, pp. 6456–6468, Nov. 2015.

[12] Z. Wang et al., "A novel magnetic coupling mechanism for dynamic wireless charging system for electric vehicles," *IEEE Trans. Veh. Technol.*, vol. 67, no. 1, pp. 124–133, Jan. 2018.

[13] J. P. K. Sampath, D. M. Vilathgamuwa, and A. Alphones, "Efficiency enhancement for dynamic wireless power transfer system with segmented transmitter array," *IEEE Trans. Transport. Electrific.*, vol. 2, no. 1, pp. 76–85, Mar. 2016.

[14] G. R. Nagendra, G. A. Covic, and J. T. Boys, "Sizing of inductive power pads for dynamic charging of EVS on IPT highways," *IEEE Trans. Transport. Electrific.*, vol. 3, no. 2, pp. 405–417, Jun. 2017.

[15] V. Z. Barsari, D. J. Thrimawithana, S. Kim, and G. A. Covic, "Modular coupler with integrated planar transformer for wireless ev charging," *IEEE Trans. Power Electron.*, vol. 38, no. 7, pp. 9206–9217, Jul. 2023.

[16] F. Lu, H. Zhang, H. Hofmann, and C. Mi, "A dynamic charging system with reduced output power pulsation for electric vehicles," *IEEE Trans. Ind. Electron.*, vol. 63, no. 10, pp. 6580–6590, Oct. 2016.

[17] C. Cai, M. Saeedifard, J. Wang, P. Zhang, J. Zhao, and Y. Hong, "A cost-effective segmented dynamic wireless charging system with stable efficiency and output power," *IEEE Trans. Power Electron.*, vol. 37, no. 7, pp. 8682–8700, Jul. 2022.

[18] W. Chen, F. Lin, and G. A. Covic, "A modified DDQ track for interoperable EV dynamic charging," *IEEE Trans. Power Electron.*, vol. 38, no. 10, pp. 11738–11750, Oct. 2023.

[19] Y. Li et al., "A new coil structure and its optimization design with constant output voltage and constant output current for electric vehicle dynamic wireless charging," *IEEE Trans. Ind Inform.*, vol. 15, no. 9, pp. 5244–5256, Sep. 2019.

[20] K. Shi, C. Tang, H. Long, X. Lv, Z. Wang, and X. Li, "Power fluctuation suppression method for EV dynamic wireless charging system based on integrated magnetic coupler," *IEEE Trans. Power Electron.*, vol. 37, no. 1, pp. 1118–1131, Jan. 2022.

[21] K. Shi, C. Tang, Z. Wang, X. Li, Y. Zhou, and Y. Fei, "A magnetic integrated method suppressing power fluctuation for EV dynamic wireless charging system," *IEEE Trans. Power Electron.*, vol. 37, no. 6, pp. 7493–7503, Jun. 2022.

[22] S. A. Al Mahmud, I. Panhwar, and P. Jayathurathnage, "Large-area free-positioning wireless power transfer to movable receivers," *IEEE Trans. Ind. Electron.*, vol. 69, no. 12, pp. 12807–12816, Dec. 2022.

[23] H. Wang, U. Pratik, A. Jovicic, N. Hasan, and Z. Pantic, "Dynamic wireless charging of medium power and speed electric vehicles," *IEEE Trans. Veh. Technol.*, vol. 70, no. 12, pp. 12552–12566, Dec. 2021.

[24] K. Lee, Z. Pantic, and S. M. Lukic, "Reflexive field containment in dynamic wireless power transfer systems," *IEEE Trans. Power Electron.*, vol. 29, no. 9, pp. 4592–4602, Sep. 2014.

[25] S. Zhou and C. C. Mi, "Multi-paralleled LCC reactive power compensation networks and their tuning method for electric vehicle dynamic wireless charging," *IEEE Trans. Ind. Electron.*, vol. 63, no. 10, pp. 6546–6556, Oct. 2016.

[26] J. M. Miller, P. T. Jones, J. Li, and O. C. Onar, "ORNL experience and challenges facing dynamic wireless power charging of EV's," *IEEE Circuits Syst. Mag.*, vol. 15, no. 2, pp. 40–53, May 2015.

[27] F. Zhao, S. Cui, C. C. Chan, and C. Zhu, "Modeling of high-efficiency non-salient pole transmitter in high-power dynamic wireless charging system for electric vehicles," *IEEE Trans. Power Electron.*, vol. 39, no. 7, pp. 8872–8882, Jul. 2024, doi: 10.1109/TPEL.2023.3321154.

[28] N. P. C. Hanspeter Widmer and L. Sieber, "Wireless power antenna alignment adjustment system for vehicles," U. S. Patent US20110254503A1, 2011.

[29] W. Zhang, J. C. White, A. M. Abraham, and C. C. Mi, "Loosely coupled transformer structure and interoperability study for EV wireless charging systems," *IEEE Trans. Power Electron.*, vol. 30, no. 11, pp. 6356–6367, Nov. 2015.

[30] C. Zhu et al., "A magnetic field concentration enhanced I-shaped transmitter for DWPT system to achieve low power fluctuation," *IEEE Trans. Power Electron.*, vol. 39, no. 1, pp. 1690–1700, Jan. 2024.

[31] B. R. Long, J. M. Miller, A. Daga, P. C. Schrafel, and J. Wolgemuth, "Which way for wireless power: High Q or high k?," in *Proc. IEEE PELS Workshop Emerg. Technol.: Wireless Power Transfer*, 2016, pp. 6–10.

[32] H. Xu, Z. Huang, X. L. Li, and C. K. Tse, "Misalignment-tolerant IPT coupler with enhanced magnetic flux variation suppression and reduced copper usage," *IEEE Trans. Power Electron.*, vol. 39, no. 8, pp. 10506–10517, Aug. 2024, doi: 10.1109/TPEL.2024.3384754.

[33] S. Li, W. Li, J. Deng, T. D. Nguyen, and C. C. Mi, "A double-sided LCC compensation network and its tuning method for wireless power transfer," *IEEE Trans. Veh. Technol.*, vol. 64, no. 6, pp. 2261–2273, Jun. 2015.

[34] T. Kan, T. D. Nguyen, J. C. White, R. K. Malhan, and C. C. Mi, "A new integration method for an electric vehicle wireless charging system using LCC compensation topology: Analysis and design," *IEEE Trans. Power Electron.*, vol. 32, no. 2, pp. 1638–1650, Feb. 2017.

Hai Xu (Graduate Student Member, IEEE) received the M.S. degree in agricultural engineering from South China Agricultural University, Guangzhou, China, in 2019. He is currently working toward the Ph.D. degree in mechanical engineering with Shien-Ming Wu School of Intelligent Engineering, South China University of Technology, Guangzhou, China.

His research interests include wireless power transfer, magnetic coupler design, magnetic modeling, and electric vehicle charging.

Zhicong Huang (Senior Member, IEEE) received the B.Eng. degree in electrical engineering and automation and the M.Eng. degree in mechanical and electronic engineering from the Huazhong University of Science and Technology, Wuhan, China, in 2010 and 2013, respectively, and the Ph.D. degree in power electronics from The Hong Kong Polytechnic University, Hong Kong, in 2018.

In 2019, he was a Postdoctoral Fellow under the UM Macao Talent Program with the State Key Laboratory of Analog and Mixed-Signal VLSI, Macau, China. Since 2020, he has been an Associate Professor with the Shien-Ming Wu School of Intelligent Engineering, South China University of Technology, Guangzhou, China. His research interests include power electronics techniques in electric vehicles and power systems.

Dr. Huang was a recipient of the Outstanding Reviewer Award from IEEE TRANSACTIONS ON POWER ELECTRONICS in 2021 and the Best Reviewer for IEEE JOURNAL ON EMERGING AND SELECTED TOPICS IN CIRCUITS AND SYSTEMS in 2023.